Pure appl. geophys. 163 (2006) 1131–1151
0033–4553/06/061131–21
DOI 10.1007/s00024-006-0067-5

Pure and Applied Geophysics

Discrete Element Modeling of Stress and Strain Evolution Within and Outside a Depleting Reservoir

HAITHAM T. I. ALASSI,[1] LIMING LI,[2] and RUNE M. HOLT[1,2]

Abstract—Stress changes within and around a depleting petroleum reservoir can lead to reservoir compaction and surface subsidence, affect drilling and productivity of oil wells, and influence seismic waves used for monitoring of reservoir performance. Currently modeling efforts are split into more or less coupled geomechanical (normally linearly elastic), fluid flow, and geophysical simulations. There is evidence (from e.g. induced seismicity) that faults may be triggered or generated as a result of reservoir depletion. The numerical technique that most adequately incorporates fracture formation is the DEM (Discrete Element Method). This paper demonstrates the feasibility of the DEM (here PFC; Particle Flow Code) to handle this problem. Using an element size of 20 m, 2-D and 3-D simulations have been performed of stress and strain evolution within and around a depleting reservoir. Within limits of elasticity, the simulations largely reproduce analytical predictions; the accuracy is however limited by the element size. When the elastic limit is exceeded, faulting is predicted, particularly near the edge of the reservoir. Simulations have also been performed to study the activation of a pre-existing fault near a depleting reservoir.

Key words: Reservoir geomechanics, numerical modeling, discrete element method, reservoir compaction, surface subsidence, stress path, fault.

Introduction

Petroleum reservoir depletion leads to stress alteration within and outside the reservoir. During recent years it has become evident that such stress changes can have a profound impact on reservoir management (e.g., TEUFEL *et al.*, 1991; ADDIS, 1997; KENTER *et al.*, 1998; HOLT *et al.*, 2004). Not only do they control purely mechanical deformation (reservoir compaction and surface subsidence), but they also impact petroleum recovery through compaction drive and through possible permeability changes. Furthermore, stress changes may affect the ability to drill stable wells, and the risks for onset of particle production or casing collapse throughout the life of the reservoir. In some cases, depletion-induced stress changes

[1]NTNU Norwegian University of Science and Technology, Trondheim, Norway. E-mail: alassi@ntnu.no; rune.holt@ntnu.no
[2]SINTEF Petroleum Research, Trondheim, Norway. E-mail: liming.li@iku.sintef.no

may be large enough to cause seismicity by activation of existing or generation of new faults. This may be utilized as a tool for reservoir performance monitoring (MAXWELL and URBANCIC, 2001). The main purpose of reservoir monitoring is to identify which parts of the reservoir that are produced, so that the production strategy can be tailored to the behavior of the reservoir. Today reservoirs are frequently monitored by "4-D" (also called time-lapse) seismic surveys. Clearly, stress sensitive wave velocities within a depleting reservoir or its surroundings may cause time-shifts that can be used as indicators of reservoir performance (KENTER *et al.*, 2004).

The economic impact of the issues above calls for modeling tools that can predict the evolution of stresses as a result of pore pressure changes associated with fluid extraction from the reservoir. Further, models need to be available that can also predict associated strains (compaction, subsidence, casing deformations), associated seismic velocity changes, and associated seismicity risk. There is currently no model that can be used to predict all these facets of the problem. Geomechanical simulators (PANDE *et al.*, 1990; ZIENKIEWICZ, 1991; JING and HUDSON, 2002) addressing large-scale problems like those described above are most often based on Finite Element (FEM) formulations, and are inherently static in the sense that they do not predict dynamic features like faulting. They do however predict plastic strain occurrence, but need to be re meshed in order to account for faulting. Although full poromechanical coupling is available (SETTARI and MOURITS, 1994; GUTIERREZ and LEWIS, 1998; LEWIS *et al.*, 2003; KOUTSABELOULIS and HOPE, 1998; OSORIO *et al.*, 1998; LONGUEMARE *et al.*, 2002) in such models, at least in a staggered manner, a further link to seismic modeling is as yet absent.

The motivation behind the work presented here is to explore the feasibility of applying an inherently dynamic model to this problem, namely a discrete element (DEM) approach. The DEM used here is the Particle Flow Code[1] (PFC), which is available in 2-D and 3-D formulations, and which has been applied with success at grain scale (CUNDALL and STRACK, 1979; POTYONDY and CUNDALL, 2004), and also has been refined to incorporate poromechanical coupling (SHIMIZU, 2004; LI and HOLT, 2004) and elastic wave propagation (LI and HOLT, 2002). Clearly, this model may have severe limitations for a reservoir or even basin-scale application as outlined here — the elements in the model can no longer be particles, but must be several meter large circular or spherical grid blocks. Conversely, the potential of the DEM to study localized failure, as demonstrated by LI and HOLT (2002), makes it attractive for the purpose of studying the impact of inelasticity which has not been properly addressed by other tools.

A key subject in reservoir geomechanics is the reservoir stress path as defined in the next Section, and how the stress path may be linked to the production strategy of

[1]Trademark of Itasca c.g., Minneapolis, U.S.A.

the field. We then proceed to describe the basic principles of the DEM used in this work (PFC). It is important to validate such an approach: Since direct experimental calibration is not possible, our validation strategy has been to determine if results of analytical elastic modeling can be reproduced. We will therefore show a comparison between predictions of the DEM and the classical Geertsma theory (GEERTSMA, 1973), both for 2-D and 3-D cases. We then proceed to address the case in which the elastic limit is exceeded somewhere in the model, leading to damage, in the form of fault generation. Finally, we demonstrate how DEM may be used to analyze the circumstances in which a pre-existing fault may be activated as a result of reservoir depletion.

Geomechanics of Depleting Reservoirs

The reservoir stress path is defined through the following parameters (HETTEMA *et al.*, 1998)

$$\gamma_v = \frac{\Delta\sigma_v}{\Delta p_f};\ \gamma_h = \frac{\Delta\sigma_h}{\Delta p_f}. \tag{1}$$

Here Δ_v and Δ_h denote vertical and horizontal stress path coefficients, representing the change in total vertical and horizontal stresses ($\Delta\sigma_v$ and $\Delta\sigma_h$) with change (Δ_{pf}) in reservoir pore pressure. Notice that the γ – parameters are valid within the reservoir as well as in the surrounding rock volume, but the pore pressure change always refers to the reservoir.

If there is no stress arching so that the full weight of the overburden is carried by the reservoir, then $\gamma_v = 0$. If in addition the reservoir compacts (linearly) elastically with no lateral strain, then

$$\gamma_h = \alpha\frac{1-2\nu_{fr}}{1-\nu_{fr}}, \tag{2}$$

where α is the poroelastic (Biot) coefficient and ν_{fr} is Poisson's ratio for the drained reservoir rock. Since $\gamma_h > 0$ and the pore pressure decrease is negative, Eqs. (1) and (2)imply that the total horizontal stress is reduced.

It is evident from field experience (TEUFEL *et al.*, 1991; ADDIS, 1997; KENTER *et al.*, 1998) and also from theoretical considerations (RUDNICKI, 1999; SEGALL and FITZGERALD, 1998) that the stress path in a general case will deviate from that above. If the reservoir is drained in such a way that the drained volume cannot be approximated as a flat "pancake"–like object, then stress arching will occur. Also, a stiff (compared to the draining rock volume) overburden will promote stress arching. One consequence of stress arching is that stress changes occur more in the overburden than within the reservoir.

GEERTSMA (1973) used the so-called "nucleus of strain" method to calculate an analytical solution for displacements as well as changes in the stress field for a depleting disk-shaped reservoir. His solution is limited by the assumption of uniform elastic properties of the sedimentary basin, including the reservoir and the surrounding rock.

In order to solve this problem for realistic field cases, where the shape of the reservoir differs from the idealized cylindrical geometry, where there is elastic contrast between the reservoir and its surroundings, and where the reservoir may be tilted, numerical techniques must be used. The Finite Element Method (FEM) has been applied to this problem by e.g. KOSLOFF *et al.* (1980); MORITA *et al.* (1989); BRIGNOLI *et al.* (1997); GAMBOLATI *et al.* (1999; 2001) and MULDERS (2003).

As an example of the outcome of such simulations, Figure 1 shows the stress path coefficients obtained on the basis of FEM simulations (MAHI, 2003) vs. depth for a case of elastic match between reservoir and surrounding rock. Results are shown for two different radii of drainage. γ_v is positive, which means that the reservoir compacts (as a response to effective stress change) less than it would if arching was not present. Outside the reservoir, where the pore pressure is not expected to change much as a result of depletion, the positive γ_v value corresponds to vertical decompression. The other stress path coefficient, γ_h, is positive within the reservoir (reduced total but increased effective horizontal stress), and negative above and below, implying horizontal compression in those areas. Reducing drainage area is

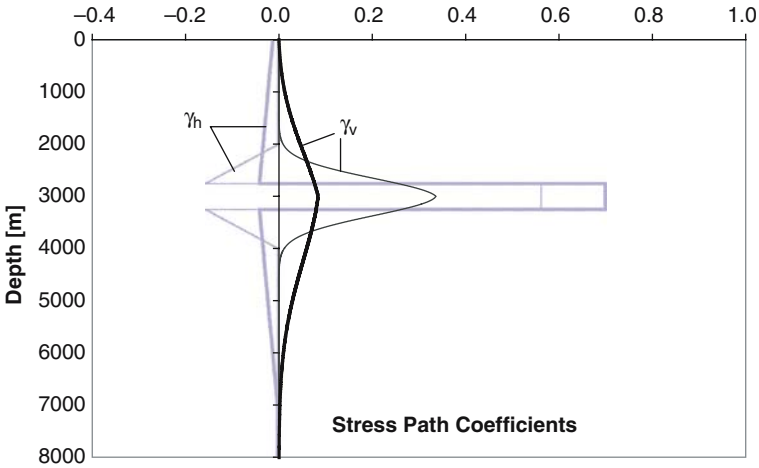

Figure 1

Vertical and horizontal stress path coefficients along a vertical line through the reservoir center, calculated based on FEM simulations (after MAHI, 2003). The computations are performed for a disk-shaped (500 m thick) reservoir centered at 3000 m depth, with a drainage radius of 2000 m (bold curves) and 500 m (narrow curves). Approximate solutions are shown for the case of elastically matched reservoir and surroundings (Young's modulus = 12 GPa; Poisson's ratio = 0.20). Notice that these curves are reproduced as mathematical approximations to FEM simulations.

seen to cause increased arching within and near the reservoir, although the influenced zone is shrinking. This situation may correspond to an early development phase or production of an isolated reservoir compartment. Note that the zone affected by stress alteration as a result of depletion in both cases extends 1000 m or more above and below the reservoir.

An important observation from FEM simulations as well as from analytical computations (SEGALL and FITZGERALD, 1998) is that the vertical stress is strongly increased near the edge on the outside of the reservoir, while the horizontal stress is reduced. This stress alteration may exceed the elastic limit of the rock around the reservoir, and the edge zone is therefore where fault generation or fault activation most likely will take place.

Discrete Element Modeling

We have in this work applied a Discrete Element Method (DEM) named PFC (''Particle Flow Code'') (CUNDALL and STRACK, 1979; POTYONDY and CUNDALL, 2004), which is widely used to model the mechanical behavior of rock and other granular materials. The material is represented by discrete particles, basically disks (in 2-D) or spheres (in 3-D) which interact with each other through a user-defined (usually linear) force-displacement contact law, using a soft contact (overlapping particles) approach. Within a calculation cycle, the values of forces and displacements are calculated, and the law of motion is applied to each particle to update position and velocity. Bonds can be inserted at the contacts to represent cementation in rocks. The model is fully dynamic, and hence able to describe complex phenomena like rock failure. One significant point in PFC is that elastic energy can be tracked during simulation, which allows the user to monitor the energy release during crack development and fault sliding. Additionally, wave propagation simulations can be easily performed (LI and HOLT, 2002) since PFC is a dynamic program.

In the subsequent sections of this paper we will use bonded models to simulate reservoir depletion and fault activation.

Elastic Case: Comparison with Geertsma's Analytical Model

Bonded particles can be used to model continuum media, similar to other numerical methods like FEM. The main purpose of the work presented in this section, is to discern to what extent PFC performs as a continuum model. To do this, a set of simulations has been performed both with two-dimensional ($PFC^{2\text{-}D}$) and three-dimensional ($PFC^{3\text{-}D}$) DEM models, and then compared to analytical predictions based on GEERTSMA (1973). Thus; the model and the boundary conditions have been constructed so that no interparticle bonds break, i.e., the model material is linearly elastic.

GEERTSMA (1973) used the center of dilatation (“nucleus of strain”) concept to calculate displacements and stress changes associated with depletion of a disk-shaped reservoir in an elastically homogeneous half-space. His analytical solutions are valid for 3-D, making it necessary to derive similar analytical solutions for the center of dilatation (represented as disks) approach in 2-D (the derivation is not shown in this paper). Also, instead of using analytical integrals as done by Geertsma for the disk-shaped reservoir, numerical integral is incorporated to solve the problem of other 3-D reservoir shapes.

Modeling of Depletion for a Rectangular Reservoir Using PFC$^{2\text{-}D}$.

PFC is suitable for grain-scale modeling, where recent studies indicate that a good qualitative and close to quantitative match between modeling and experiment can be obtained (HOLT *et al.*, 2005). Since here we use PFC for modeling of large-scale behavior, the particle size must be chosen large (typically 20 m radius in this work) as well, to keep reasonable computational time. No controlled experiment is possible, consequently, validation is performed by comparison with an analytical model as described above.

In order to make the PFC model most comparable to continuum models, the particle packing should be chosen as compact as possible. In the work presented here, a hexagonal packing of uniformly-sized particles is used. This leads to anisotropy, which creates difficulty in finding suitable linear elastic parameters for the model when comparing it to isotropic analytical theory. An alternative would be to choose a

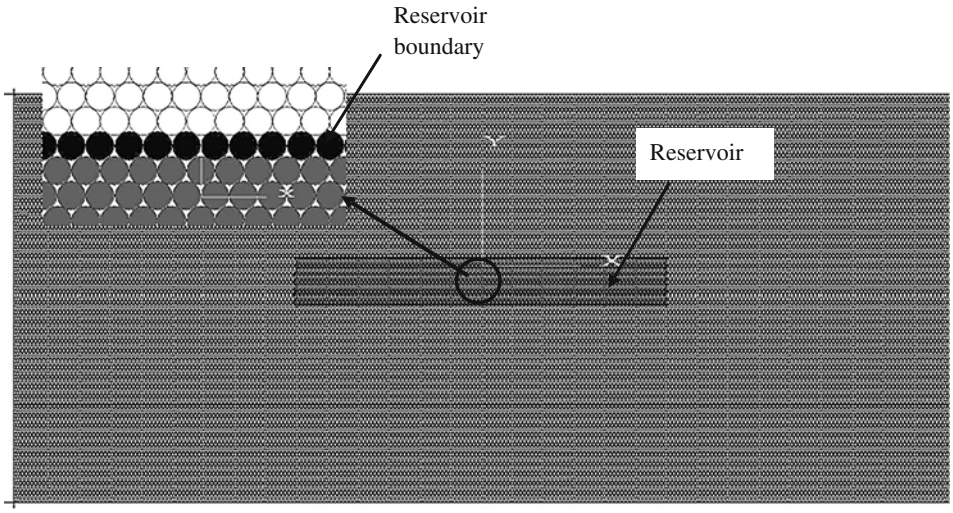

Figure 2
PFC$^{2\text{-}D}$ geomechanical model used for modeling reservoir depletion. The black particles along the reservoir boundary denote where forces are applied to simulate depletion.

broad particle-size distribution. Further, force transmission in granular materials is different from that in continua. The force chain pattern depends not only on the elastic parameters of the system, but also on the contact law that governs the relation among the neighboring particles (linear or nonlinear), and the packing of the particles.

The model is 10 km wide and 4.3 km deep. It is composed of a hexagonal packing of 31250 equally sized (radius = 20 m) particles. After packing, gravitational force is added under zero lateral strain (fixed walls) boundary conditions. Finally, parallel bonds are inserted at all interparticle contacts. The tensile as well as the shear strength of the bonds are set equal to 5 MPa. Figure 2 shows the model that is used during the simulation, including a rectangular reservoir inserted at 2000 m depth from the surface. Table 1 shows the model properties. Note that the reservoir parameters do not represent any real reservoir, since the main purpose of this study is to demonstrate feasibility of DEM for reservoir and basin scale studies.

The reservoir is depleted uniformly, with no drainage to the surroundings. Under this assumption, the pore pressure gradient on the boundary will be very large, whereas inside the reservoir it will be zero. In FEM modeling this problem may be solved using a technique presented by GAMBOLATI *et al.* (2001). They let the pore pressure decrease from p_f to zero on a string of elements around the reservoir. In our model we similarly apply these forces to all particles at the reservoir boundary. The accuracy of our solution will hence depend on the element (i.e., particle) size, which is linked to computational time.

Using this method, the reservoir is depleted by a pore pressure change $\Delta p_f = -10$ MPa. The reservoir has been placed at different depths c within the model basin. Young's modulus and Poisson's ratio of the reservoir material (as listed in Table 1) were determined by performing a biaxial test on a sample with the same PFC parameters as the reservoir. In the reservoir model there is however a stress gradient, therefore elastic parameters are also expected to change with depth. No bonds were broken in the model during this simulation, meaning that the PFC material behaves perfectly elastic. The resulting compaction and subsidence are plotted in Figure 3 together with the analytical solution obtained from Geertsma's

Table 1

Model properties for the PFC$^{2\text{-}D}$ simulations

Properties	Values
Model dimensions [km]	10 * 4.3
Reservoir dimension [m]	4000*500
Particle radius [m]	20
Interparticle normal stiffness [GN/m]	24
Interparticle shear stiffness [GN/m]	12
Interparticle normal and shear bond strength [MPa]	5
Young's modulus [Gpa]	30
Poisson's Ratio [-]	0.14

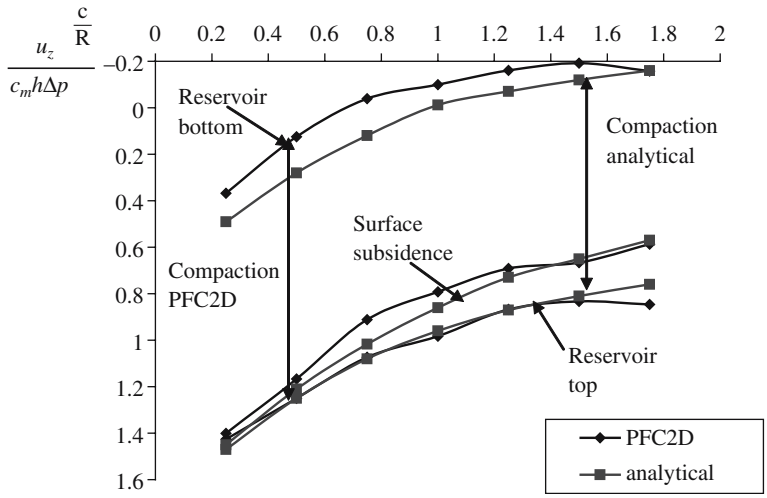

Figure 3

Surface subsidence and displacement at the top and the bottom of a rectangular (4000 × 500 m) reservoir, simulated with a PFC$^{2\text{-D}}$ model and those obtained by analytical solution. Results are shown for different reservoir depths. The reservoir is depleted with Δp_f 10 MPa. u_z is the vertical displacement, c_m is the uniaxial compaction coefficient, h, R, and c are reservoir thickness, radius (= 2000 m), and depth, respectively. Reservoir compaction equals the difference between reservoir top and bottom displacements.

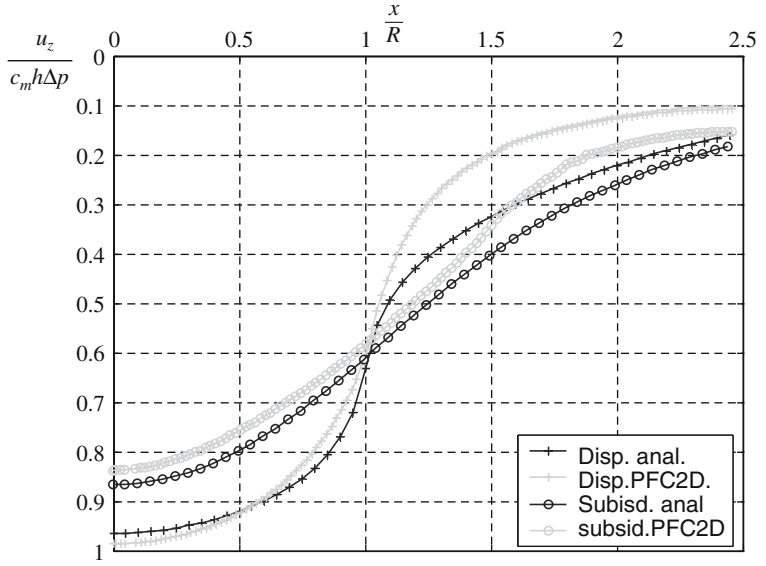

Figure 4

Comparison between PFC$^{2\text{-D}}$ modeled and analytically calculated reservoir displacement (at the top of the reservoir) and surface subsidence along the x axis (lateral direction). Model parameters are listed in Table 1, reservoir depth is 2000 m, *uz* is the vertical displacement. cm is the uniaxial compaction coefficient, *h* is reservoir thickness, *R* is the reservoir radius.

method, adapted to 2-D. As depth c increases, the values of subsidence and also the displacement of the top of the reservoir decrease, given that the reservoir dimensions are kept unchanged. It can also be seen that for shallow depths ($c/R < 0.5$; R is reservoir radius) the value of subsidence becomes closer to that of vertical displacement at the top of the reservoir. Satisfactory agreement is obtained between the numerical and the analytical solutions. Figure 4 shows a similar comparison between PFC$^{2\text{-D}}$ and the Geertsma 2-D solution of the subsidence and compaction bowls in the case of a reservoir placed at 2000 m depth. The agreement is again acceptable.

The PFC$^{2\text{-D}}$ simulation permits determination of the stress path coefficients (Eq. (1)) throughout the model. The changes in vertical and horizontal stresses are measured after depleting the reservoir by 10 MPa. The arching coefficients obtained from PFC and analytical solutions are shown vs. depth through the reservoir center in Figure 5, and in the lateral direction just above the top of the reservoir in Figure 6. Note that the discrete element model predicts an increase in the horizontal stress path coefficient with distance from the center of the reservoir towards the edge, as was found also in the finite-element simulations of a disk-shaped reservoir by MULDERS (2003). On the other hand, there is a significant difference between the results of the PFC simulation and the analytical solution: While the trends are the same, the values

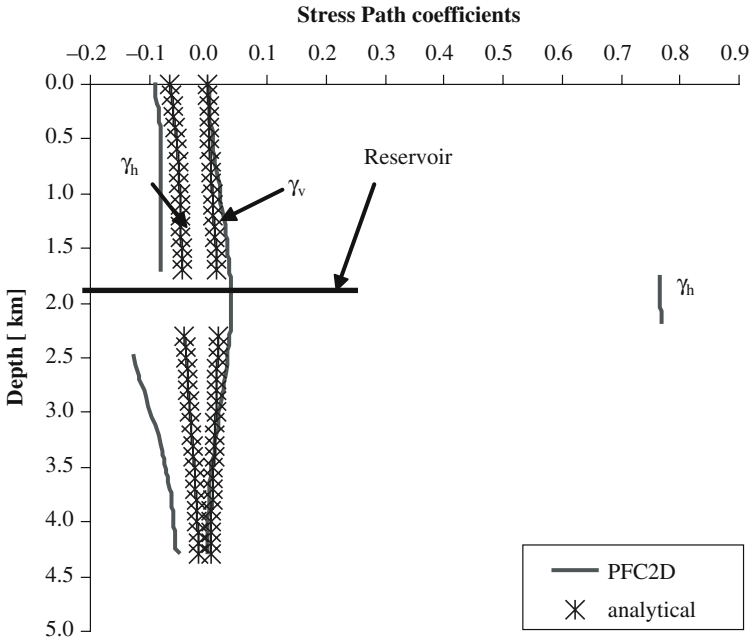

Figure 5
Vertical and horizontal arching coefficients versus depth, from PFC$^{2\text{-D}}$ simulation. Reservoir depth = 2000 m.

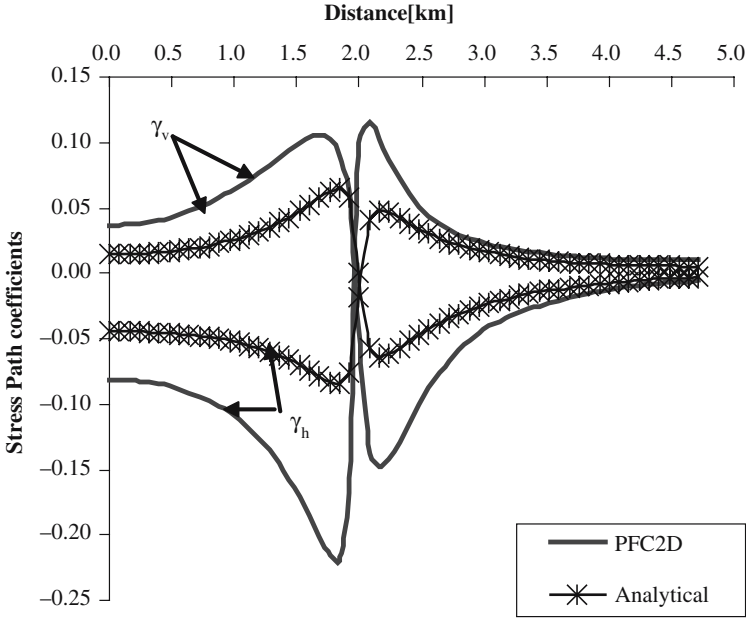

Figure 6
Vertical and horizontal arching coefficients along x axis, from PFC$^{2\text{-}D}$ simulation. Reservoir depth = 2000 m.

of the stress path coefficients differ significantly. This is related to element size and texture as mentioned above, and particularly to choosing the appropriate elastic parameter for the analytical computation. The difference also depends on the method used to measure the stress in PFC: To date the stress is assumed to exist only in the particles (or disks). The boundary conditions also highly contribute to the difference, as can be seen in Figure 4, where the discrepancy between the analytical and the numerical solution increases with distance from the reservoir boundary towards the model boundary.

Table 2

Model properties for the PFC$^{3\text{-}D}$ simulations

Properties	Values
Model dimensions [m]	1600 * 1600*800
Reservoir dimension [m]	800*800*120
Particle radius [m]	20
Young's modulus [GPa]	12
Poisson's Ratio [-]	0.0

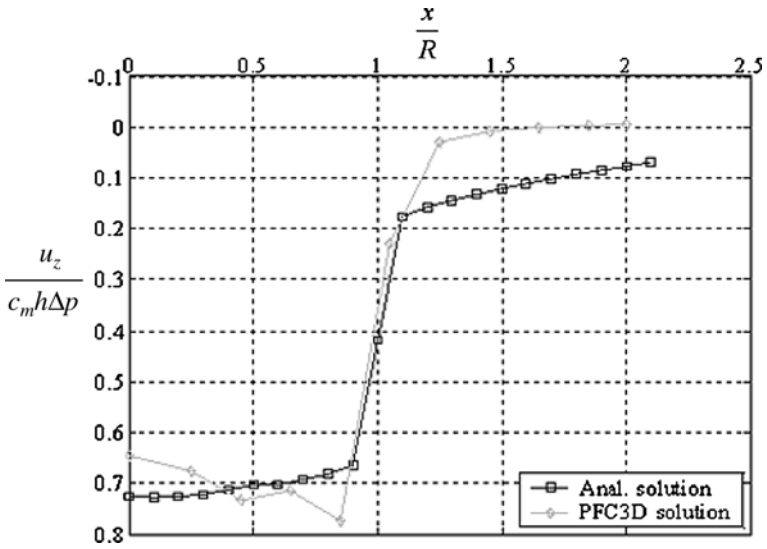

Figure 7
Comparison between PFC$^{3\text{-D}}$ modeled and analytically calculated (with the nucleus of strain model; GEERTSMA, 1973) compaction (at the top of the reservoir). Model parameters are listed in Table 2, reservoir depth is 400 m.

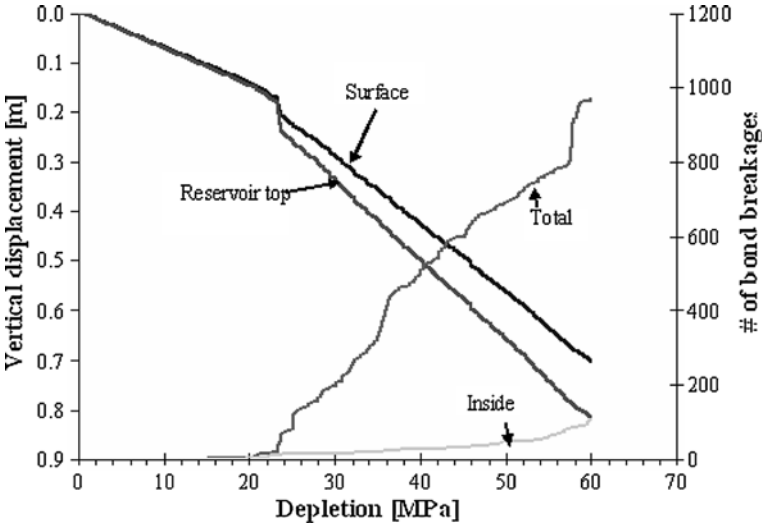

Figure 8
Vertical displacements at the surface and at the top of the reservoir during simulated depletion, using a PFC$^{2\text{-D}}$ model as described in the text. Also shown are recorded numbers of broken bonds between elements within the reservoir and in the full model.

Modeling of Depletion Using PFC$^{3\text{-}D}$

A PFC$^{3\text{-}D}$ model consisting of 32,000 spherical particles is constructed, using a cubic packing (see Table 2 for model description). The element (particle) size was kept the same as in the 2-D modeling (20 m). In order to limit computational time, the model size is considerably reduced ($1600 \times 1600 \times 800$ m). The reservoir thickness is 120 m, and it is inserted at a depth of 400 m. Depletion of the reservoir is again simulated by applying normal forces to the boundary particles (as was done above).

Figure 7 shows a comparison between PFC$^{3\text{-}D}$ modeling and the Geertsma [3-D] solution for compaction at the top of the reservoir. Again, a triaxial test was performed to establish Young's modulus and Poisson's ratio for the reservoir material. As in the 2-D case, the fit is acceptable, but not perfect. The reasons for not accomplishing perfect matching are the same as above: The size of the model relative to the particle size is even smaller in this case, which is a primary source of error. Again; rock properties in the PFC model are expected to vary with depth, and the cubic packing also introduces a slight anisotropy. Nevertheless, a main conclusion is that both 2-D and 3-D PFC simulations with perfectly elastic (no bond breakage) material produce results which are fairly close to analytical predictions.

Beyond Elasticity: Fault Initiation within and outside a Depleting Reservoir

As can be depicted from the previous sections, the stresses evolving during reservoir depletion may exceed the elastic limit; within the reservoir, as well as outside of it. This may lead to the formation of localized deformation bands, or activation of pre-existing faults. In order to study faulting, the PFC$^{2\text{-}D}$ model created in the previous section was used, with a significantly larger reservoir depletion (= 60 MPa).

Figure 8 shows the modeled surface subsidence and displacement at the top of the reservoir. The rate of compaction increases with increasing depletion, and the increased reservoir compressibility can be directly linked to damage inside the reservoir as measured by the number of bond breakages. The vertical displacement on the surface of the model shows a similar trend. Obviously, the increased compaction within the reservoir contributes to this. The change in subsidence to compaction ratio is small, in spite of significant bond breakage also in the surrounding material, in particular near the reservoir edges, as illustrated in Figure 9. The localized failure zone near the reservoir edge seems to have little impact on the surface subsidence, at least as long as they do not reach the surface. The observed failure pattern is in agreement with expectations based on analytical computations, finite-element simulations (e.g., BRIGNOLI *et al.*, 1997), as well as laboratory modeling (PAPAMICHOS *et al.*, 2001). While bonds fail largely in shear within the reservoir, tensile bond failures dominate outside. This is partly a result of the somewhat arbitrary choice of tensile vs. shear bond strengths. Notice that

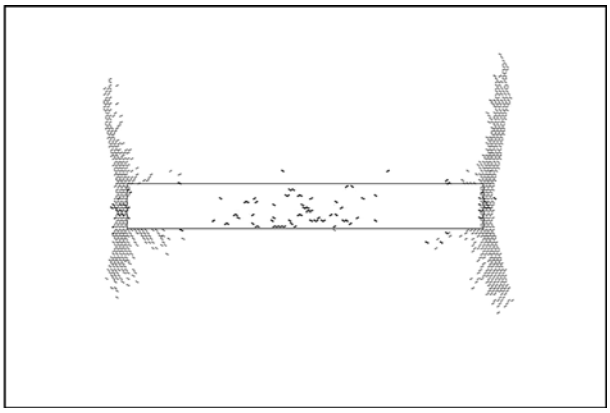

Figure 9
Positions of bond breakages after depleting the PFC$^{2\text{-}D}$ model shown in Figure 2 with 60 MPa. The black line segments indicate local shear failures, while the grey ones represent tensile failures.

the failure pattern in this simulation corresponds largely to that seen in a previous PFC$^{2\text{-}D}$ simulation (HOLT *et al.*, 2004), but differs in details: In that case, significant bond breakage occurred above the reservoir as well as near the edges. The difference is mainly caused by the difference in particle-size distribution and texture. Figure 10 also shows bond breakages after continued depletion to 100 MPa (notice that the values are arbitrarily chosen and do not represent a real case — in reality, the level of depletion should be compared to the strength parameters of the surrounding and reservoir rock). Cracks are seen to propagate to

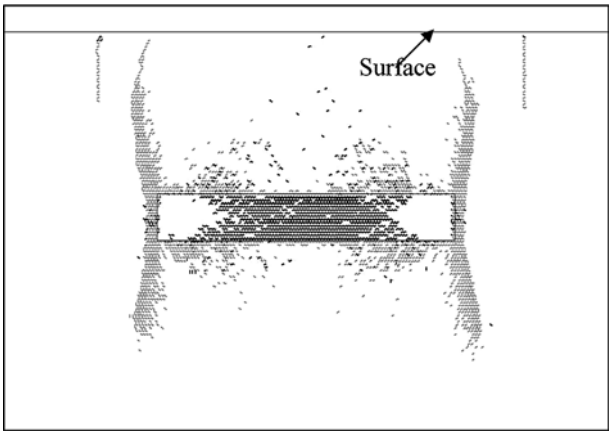

Figure 10
Positions of bond breakages after depleting the PFC$^{2\text{-}D}$ model shown in Figure 2 with 100 MPa. The black line segments indicate local shear failures, while the grey ones represent tensile failures.

the surface and the number of cracks inside and outside the reservoir increase significantly. Although this is not a realistic case, it shows a similar trend to that obtained from laboratory modeling (PAPAMICHOS *et al.*, 2001).

DEM Modeling with a Pre-existing Fault

The simulations shown in the previous section demonstrate that the DEM is able to simulate faulting during depletion of an initially intact reservoir embedded in initially intact surroundings. One may however question if this fault pattern is realistic or not – it is clearly limited by the resolution of the simulation (particle size), which limits the possibility for a fault to localize within the model. In reality, faults may also exist before the reservoir is depleted. The positions of these faults may be seen from seismics, and then it makes no sense to use a numerical model to attempt reproduction of their formation.

These considerations triggered a study of how PFC may be used to embed and simulate the behavior of an existing fault, and to explore the feasibility of studying fault response to reservoir depletion.

To create a fault in PFC$^{2\text{-}D}$, the same model as in previous sections is applied, but with specific properties assigned to a group of particles along a pre-defined fault plane. Table 3 presents the fault properties. Recognize that since the hexagonal packing is used, the fault takes a straight shape because of the chosen dipping angle (60°). Irregular packing may also be used, however then smaller particle sizes need to be created in the fault zone. Slip may be initiated in different ways. A triggering process driven by a high shear stress is mimicked by reducing the friction coefficient between the fault particles and neighboring particles. If the process is triggered by high normal stress, fault activation may be simulated by slightly reducing the size (by 1%) and stiffness (see Table 3) of the fault particles.

After the fault is initiated, the model is run to equilibrium, where the unbalanced force is reduced to a minimum value, and no further fault slipping occurs. In our case, a normal fault is developed according to both scenarios above, since the model

Table 3

Fault properties used in PFC simulations. These properties are assigned to all the particles that compose the fault

Properties	Values
Normal stiffness k_n [GN/m]	1
Shear stiffness k_s [GN/m]	0.5
Friction coefficient μ [-]	0.3
Fault length [m]	1480
Fault dip angle [°]	60

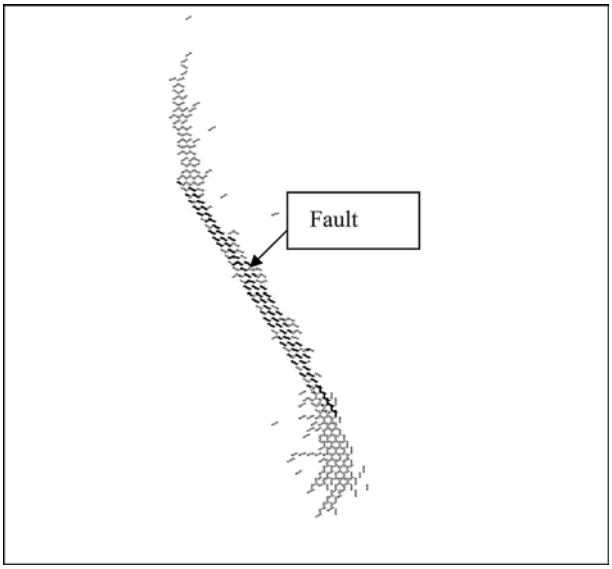

Figure 11
Bond breakages during fault sliding, triggered by reducing the interparticle friction coefficient. Note that all bond failures are tensile (gray color), except at the fault face, which shows failures in shear (black).

is in a normal-faulting environment (vertical > horizontal stress). The hanging wall slips downward and the foot wall slips upward.

The shear-induced fault (Fig. 11) extends in the direction of the maximum principal stress by development of wing cracks. Damage is mainly located of the tip

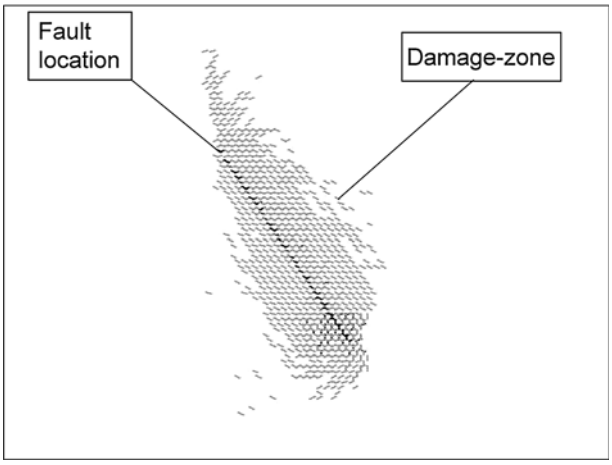

Figure 12
Bond breakages during fault sliding, triggered by reducing particle size and stiffness. Note that all bond failures are tensile (gray color), except at the fault face, which shows failures in shear (black).

regions of the fault. The compaction-induced fault, on the other side, develops a more extended damage zone (Fig. 12).

Fault sliding alters the stress distribution of the model, leading to stress concentrations at the tips of the fault. On one side of the tip, the stress increases (more compression), while on the other side of the same tip, there is an area where the stress decreases (becomes more tensile). Within the stress reduction zones, bonds may break in tension. Cracks grow during sliding of the fault as a result of more stress concentration, and the stress re-distribution caused by bonds breakage. Eventually the cracks that nucleate at different places will coalesce with each other forming a damage-zone around the fault. The cracks do not only start at the tips of the fault, but also along the fault plane, because of the stress disturbance caused by a sudden change of the stiffness and the size of the particles that form the fault. Figure 12 shows the tensile breakages of the parallel bonds at the end of the simulation. ODED *et al.* (2002) presented a fault deformation model which predicts damage (cracks) not only at the fault tips, but also along the fault plane, as is also seen from the PFC model with particle shrinkage as the fault trigger.

Reservoir Depletion, with Fault on the Side of the Reservoir

To study the effect of reservoir depletion on re-activation of a fault, a reservoir is inserted to the left of the fault created previously (see Fig. 13). The size of the reservoir is (arbitrarily chosen) 2500 *500 m. Again an undrained boundary condition is assumed. According to SEGALL and FITZGERALD (1998), normal faults that lie on the side of the reservoir will be re-activated under such circumstances,

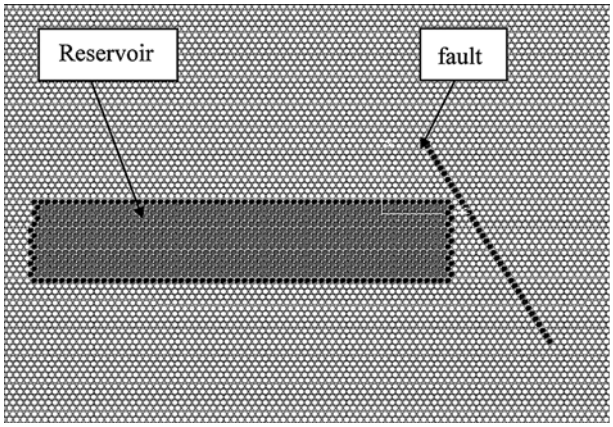

Figure 13
A normal fault is placed to the right of a reservoir. The model is used to simulate the re-activation behavior of the fault due to reservoir depletion.

given a sufficient pore pressure reduction. A simulated reservoir depletion of 40 MPa causes slipping of the fault, the hanging wall moves downward, while the foot wall follows the movement of the reservoir boundary. It can be seen that the deformation of the lower boundary increases the amount of slip, while the deformation of the upper boundary of the reservoir decreases the slip between the two fault faces. This behavior differs from that of a typical normal fault, in which the foot wall is expected to move upward.

The slip or frequently called RSD (relative shear displacement) is plotted in Figure 14 versus depth after 20 and 40 MPa depletion. This value represents the relative displacement between the two sides of the fault in the dipping direction. Reactivation causes new bond breakage in the area of stress concentration; in this case at the tensional side of the fault tips. Figure 15 depicts the new cracks that are developed due to reservoir depletion. The increasing tension on the sides of the reservoir as a result of depletion causes creation of a tensile-normal fault in the direction perpendicular to minimum horizontal stress (SEGALL and FITZGERALD, 1998; FERRILL and MORRIS, 2003). Since in our model the minimum stress is horizontal, the created tensile fault has a dip angle = 0 (vertical fault).

Discussion

The simulations presented here demonstrate the feasibility of using a discrete element model to simulate the geodynamics of a depleting reservoir. The strength of

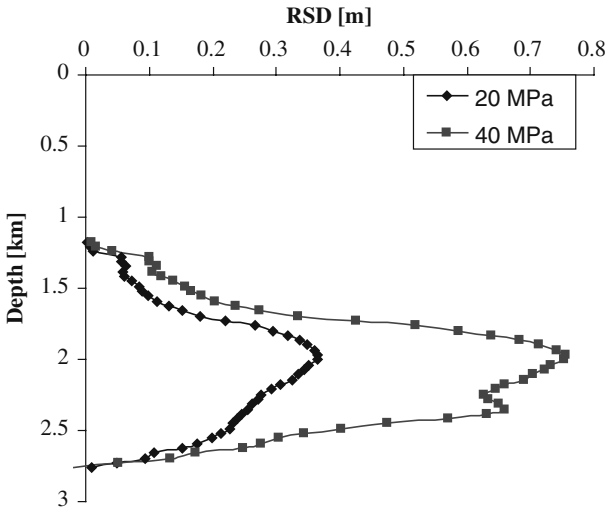

Figure 14
Slip between the fault faces (see Fig. 12) after 20 and 40 MPa depletion.

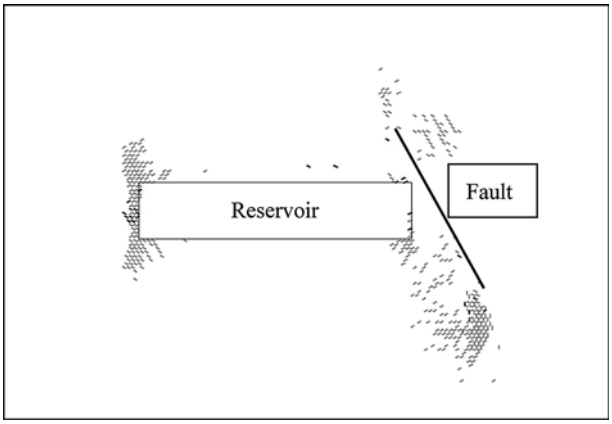

Figure 15
Bond breakages developed after depleting the reservoir in Figure 12 by 40 MPa. Note the concentration of the cracks at the tips of the fault and also at tips of the reservoir, as a result of stress concentration in those areas.

DEM is the ability to simulate faulting and fault activation in a dynamic manner, where natural complexity emerges from simple contact laws. A dynamic approach is therefore beneficial when fracturing is expected to take place. Consequently traditional finite-element solutions suffer, mainly from the need to continuously remesh as a fracture grows, but also because of limitations in path conformability and element size. However; there will be a multitude problems where FEM solutions are sufficient, and these solutions are more efficiently obtained than DEM solutions.

Element size also is a main restriction for DEM. Within limits of current computer technology, element size cannot be reduced to the size of physical particles. Rules need to be developed to guide the choice of particle size distribution and packing, and to guide the choice of parameters for contact laws between elements. Notice that disks or spheres as used here are basic building blocks which may be grouped into clusters or ''clumps'' to generate elements of various shapes (POTYONDY and CUNDALL, 2004; LI and HOLT, 2002). Micromechanical calibration (as in HOLT *et al*., 2005) cannot be expected to provide a complete answer here, and the approach must be based largely on field experience, geological considerations, and comparison to theory or other modeling tools. Improved resolution may however be obtained by using small particles in parts of the model where the dynamic feature is most required. This may be achieved with PFC by utilizing a recent option for automatic linkage of the DEM to a continuum (e.g., FEM or finite-difference) model.

In the PFC simulations shown here, poromechanical coupling was (for simplicity) not applied. This is however possible (SHIMIZU, 2004; LI and HOLT, 2004), and would permit more realistic treatments of pressure gradients within a reservoir compartment

and across faults. This also permits well drainage to be part of the model. Currently, only single phase fluid flow has been coupled to PFC, nonetheless this is not a fundamental limitation. Also, since wave propagation can be performed relatively easy with PFC (LI and HOLT, 2002), direct simulations of seismic surveys as well as induced seismicity (HAZZARD and YOUNG, 2000) may be incorporated within the same scheme as the geomechanical and fluid flow simulations.

Conclusions

We have demonstrated the feasibility of a Discrete Element Model (PFC) to simulate stress evolution and associated displacements resulting from pore pressure depletion of a producing reservoir. The model was calibrated in 2-D as well as 3-D for a case of perfect elasticity, when comparison could be made to analytical calculations by the nucleus of strain theory (GEERTSMA, 1973). The accuracy of the DEM is limited by element size, which here was 20 m (given by the radius of disk elements in 2-D; spheres in 3-D). While calculated compaction and subsidence were in good agreement with theory, the scatter in stress calculations was more significant. The results are also sensitive to particle size distribution and packing, indicating that more work is required to optimize the choices of these parameters and parameters controlling the contact law between particles. Also as with other numerical methods, the results are largely affected by the boundary conditions. Therefore the model must be refined to achieve better results.

The simulations performed illustrate the ability of the DEM to generate localized faults when the elastic limit is exceeded somewhere in the model. As one would expect from analytical stress calculations and from previous numerical work, faulting is likely to take place in the surrounding near the edge of a depleting reservoir. When faults are known to exist prior to depletion and can be identified from seismic images, they may be embedded in the DEM model by selecting an array of particles with properties different from the surroundings. In our case, two options for numerical simulation of fault activation were considered; (i) reduced friction; (ii) reduced particle size and stiffness. Further work is required to find a geologically representative formulation for a fault in the DEM.

We conclude that DEM, such as PFC, may provide useful insight into the dynamic behavior of a rock mass such as in the case of a depleting reservoir embedded in a sedimentary basin. In principle, fluid flow and elastic wave propagation may also be incorporated in this model. Only when faulting is expected to take place will DEM be beneficial compared to more traditional simulation approaches (like FEM). Improvements include reducing particle (element) size, particularly in zones where failure may occur. Linking of DEM to a continuum model appears to be a promising tool for this.

Aknowledgement

The authors acknowledge the Norwegian Research Council for financial support to this work through the Strategic University Program "ROSE – Improved Overburden Characterization combining Seismics and Rock Physics" at NTNU (Norwegian University of Science and Technology).

References

Addis, M.A. (1997), *The stress-depletion response of reservoirs*, SPE 38720, 11 pp.

Brignoli, M., Pellegrino, A., Santarelli, F.J., Musso, G. and Barla, G. (1997), *Continuous and discontinuous deformations above compacting reservoirs; consequences upon the lateral extension of the subsidence bowl*, Int. J. Rock Mech. and Min. Sci. *34* (3–4).

Cundall, P.A. and Strack, O.D.L. (1979), *A discrete numerical model for granular assemblies*, Géotechnique *29*(1), 47–65.

Gambolati, G., Teatini, P., and Tomasi, L. (1999) *Stress-strain analysis in productive gas/oil reservoirs*, Int. J. Numer. Anal. Meth. Geomech. *23*, 1495–1519.

Gambolati, G., Ferronato, M., Teatini, P., Deidda, R., and Lecca, G. (2001), *Finite element analysis of land subsidence above depleted reservoirs with pore pressure gradient and total stress formulations*, Int. J. Numer. Anal. Meth. Geomech. *25*, 307–327.

Gutierrez, M. and Lewis, R.W. (1998), *The role of geomechanics in reservoir simulation*, SPE/ISRM 47392. In Proc. EUROCK'98, vol. II, pp. 439–448.

Geertsma, J. (1973), *A basic theory of subsidence due to reservoir compaction: The homogeneous case*, Trans. Royal Dutch Soc. Geol. and Mining Eng. *22*, 43–62.

Hazzard, J.F. and Young, R.P. (2000), *Simulating acoustic emissions in bonded-particle models of rock*, Int. J. Rock Mech. and Min. Sci. *37*, 867–872.

Hettema, M.H.H., Schutjens, P.M.T.M., Verboom, B.J.M., and Gussinklo, H.J. (1998), *Production-induced compaction of sandstone reservoirs: The strong influence of field stress*, SPE50630, 8 pp.

Holt, R.M., Flornes, O., Li, L., and Fjær, E. (2004), *Consequences of depletion-induced stress changes on reservoir compaction and recovery*, In Proc. Gulf-Rock (eds. Arma/Narms) 04–589, ARMA/NARMS, 10 pp.

Holt, R.M., Kjølaas, J., Larsen, I., Li, L., Pillitteri, A.G., and Sønstebø, E.F. (2005) *Comparison between controlled laboratory experiments and discrete particle simulations of rock mechanical behaviour*, Int. J. Rock Mech. and Min. Sci. *42*, 985–995.

Jing, L. and Hudson, J.A. (2002), *Numerical methods in rock mechanics*, Int. J. Rock Mech. and Min. Sci. *39*, 409–427.

Kenter, C.J., Blanton, T.L., Schreppers, G.M.A., Baaijens, M.N. and Ramos, G.G. (1998), *Compaction study for Shearwater Field*, SPE/ISRM 47280. In Proc. EUROCK'98; Vol. II, pp. 63–68.

Kenter, C.J., Beukel, A. v. d., Hatchell, P., Maron, K. and Molenaar, M. (2004), *Evaluation of reservoir characteristics from timeshifts in the overburden*, In Proc. Gulf-Rock (eds. Arma/Narms) 04–627, ARMA/NARMS.

Kosloff, D., Scott, R.F., and Scranton, J. (1980), *Finite element simulation of Wilmington oil field subsidence: 1. Linear modelling*, Tectonophysics *65*, 339–368.

Koutsabeloulis, N.C. and Hope, S.A. (1998) *"Coupled" stress / fluid / thermal multi-phase reservoir simulation studies incorporating rock mechanics*, SPE/ISRM 47393. In Proc. EUROCK'98 Vol. II, pp. 449–454.

Lewis, R.W., Makurat, A. and Pao, K.S. (2003), *Fully coupled modeling of subsidence and reservoir compaction of North Sea oil fields*, Hydrogeology J. *11*, 142–161.

Li, L. and Holt, R.M. (2002), *Particle scale reservoir mechanics*, Oil and Gas Science and Technology - Revue de l'Institut Français du Pétrole *57*, 525–538.

Li, L. and Holt, R.M., *A study on the calculation of particle volumetric deformation in a fluid coupled PFC model*, In *Numerical Modeling in Micromechanics via Particle Methods – 2004* (eds. Shimizu, Hart and Cundall) (A. A. Balkema 2004) pp. 273–279.

LONGUEMARE, P., MAINGUY, M., LEMONNIER, P., ONAISI, A., and GÉRARD, C. (2002), *Geomechanics in reservoir simulation: Overview of coupling methods and field case study*, Oil and Gas Science and Technology - Revue de l'Institut Français du Pétrole *57*, 471–483.

MAHI, A. (2003), *Stress path of depleting reservoirs*, MSc Thesis, NTNU (Norwegian University of Science and Technology).

MAXWELL, S.C. and URBANCIC, T. (2001), *The role of passive microseismic monitoring in the instrumented oil field*, The Leading Edge, 636–639.

MORITA, N., WHITFILL, D.L., NYGAARD, O., and BALE, A. (1989), *A quick method to determine subsidence, reservoir compaction, and in-situ stress induced by reservoir depletion*, JPT Jan.89, pp. 71–79.

MULDERS, F.M.M. (2003), *Modelling of stress development and fault slip in and around a producing gas reservoir*, Ph.D. Thesis, TU Delft, Netherlands.

ODED, K., ZE'EV, R., and GIDON, B. (2003), *Faults and their associated host rock deformation: Part I. Structure of small faults in a quartz–syenite body, southern Israel*, J. Struct. Geol. *25*, 1675–1689.

OSORIO, J.G., CHEN, H-Y., TEUFEL, L.W. and SCHAFFER, S. (1998), *A two-domain, 3-D, fully coupled fluid-flow / geomechanical simulation model for reservoirs with stress-sensitive mechanical and fluid-flow properties*, SPE/ISRM 47397. In Proc. EUROCK'98, Vol. II, pp. 455–464.

PANDE, G.N., BEER, G. and WILLIAMS, J.R., *Numerical Methods in Rock Mechanics* (Wiley 1990).

PAPAMICHOS, E., VARDOULAKIS, I., and HEIL, L.K. (2001), *Overburden modeling above a compacting reservoir using a trap door apparatus*, Phys. Chem. Earth (A) *26*, 69–74.

POTYONDY, D.O. and CUNDALL, P.A. (2004), *A bonded particle model for rock*, Int. J. Rock Mech. and Min. Sci. *41*, 1329–1364.

RUDNICKI, J.W. (1999), *Alteration of regional stress by reservoirs and other inhomogeneities: Stabilizing or destabilizing?* Proc. Int. Congress on Rock Mechanics (eds. G. Vouille and P. Berest), ISRM, Vol. 3; pp. 1629–37.

SEGALL, P. and FITZGERALD, S.D. (1998), *A note on induced stress changes in hydrocarbon and geothermal reservoirs*, Tectonophysics *289*, 117–28.

SETTARI, A. and MOURITS, F.M. (1994) *Coupling of geomechanics and reservoir simulation models*, Computer Methods and Advances in Geomechanics, 2151–2158.

SHIMIZU, Y., *Fluid coupling in PFC$^{2\text{-}D}$ and PFC$^{3\text{-}D}$. In Numerical Modeling in Micromechanics via Particle Methods – 2004* (eds. Shimizu, Hart and Cundall) (A. A. Balkema 2004), pp. 281–287.

TEUFEL, L.W., RHETT, D.W., and FARRELL, H.E. (1991), *Effect of reservoir depletion and pore pressure drawdown on in situ stress and deformation in the Ekofisk field*. In *Rock Mechanics as a Multidisciplinary Science* (ed. J.C. Roegiers) (A.A. Balkema 1991), pp. 63–72.

ZIENKIEWICZ, O.C., *The Finite Element Method in Engineering Geoscience* (4th edition). (McGraw-Hill 1991).

(Received April 5, 2005, revised September 19, 2005, accepted October 6, 2005)